Heliyon 10 (2024) e27361

Contents lists available at ScienceDirect

Heliyon

journal homepage: www.cell.com/heliyon

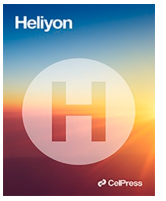

Research article

Identification of bioactive compounds of *Zanthoxylum armatum* as potential inhibitor of pyruvate kinase M2 (PKM2): Computational and virtual screening approaches

Mohd Afzal [a,*], Faizan Abul Qais [b], Naaser A.Y. Abduh [a], Maria Christy [c], Rashid Ayub [d], Abdullah Alarifi [a]

[a] Department of Chemistry, College of Science, King Saud University, Riyadh, 11451, Saudi Arabia
[b] Department of Agricultural Microbiology, Faculty of Agricultural Sciences, Aligarh Muslim University, Aligarh, UP, 202002, India
[c] Department of Energy Engineering, Hanyang University, 222 Wangsimni-ro, Seongdong-gu, Seoul, 04763, South Korea
[d] Department of Science Technology and Innovation, King Saud University, Riyadh, 11451, Saudi Arabia

ARTICLE INFO

Keywords:
PKM2
Zanthoxylum armatum
Virtual screening
Anticancer
Molecular dynamics simulation

ABSTRACT

PKM2 (Pyruvate kinase M2) is the isoform of pyruvate kinase which is known to catalyse the last step of glycolysis that is responsible for energy production. This specific isoform is known to be highly expressed in certain cancerous conditions. Considering the role of this protein in various cancer conditions, we used PKM2 as a target protein to identify the potential compounds against this target. In this study, we have examined 96 compounds of *Zanthoxylum armatum* using an array of computational and in silico tools. The compounds were assessed for toxicity then their anticancer potential was predicted. The virtual screening was done with molecular docking followed by a detailed examination using molecular dynamics simulation. The majority of the compounds showed a higher probability of being antineoplastic. Based on toxicity, predicted anticancer potential, binding affinity, and binding site, three compounds (nevadensin, asarinin, and kaempferol) were selected as hit compounds. The binding energy of these compounds with PKM2 ranged from −7.7 to −8.3 kcal/mol and all hit compounds interact at the active site of the protein. The selected hit compounds formed a stable complex with PKM2 when simulated under physiological conditions. The dynamic analysis showed that these compounds remained attached to the active site till the completion of molecular simulation. MM-PBSA analysis showed that nevadensin exhibited a higher affinity towards PKM2 compared to asarinin and kaempferol. These compounds need to be assessed properties in vivo and in vitro to validate their efficacy.

1. Introduction

Cancer is one of the leading causes of death and a significant barrier to life expectancy Worldwide. There are several methods for managing and treating cancer, including surgery, chemotherapy, radiation therapy, and combinations of these [1]. Surgery and radiation treatments are successful yet uncomfortable for cancer many patients. Chemotherapies usually have side effects, and certain tumours are chemotherapy resistant. A major demand in public health is the discovery of clinically effective anticancer medications

* Corresponding author.
E-mail address: maslam1@ksu.edu.sa (M. Afzal).

https://doi.org/10.1016/j.heliyon.2024.e27361
Received 30 September 2023; Received in revised form 26 February 2024; Accepted 28 February 2024
Available online 5 March 2024

that can specifically target cancer cells while being safe for healthy cells. One interesting approach is to look for natural compounds that have cancer cell-specific cytotoxicity. Since ancient time, natural substances derived from plants and marine organisms have the potential to serve as effective anticancer medications [2–4]. Warburg discovered that abnormal glucose metabolism is a key characteristic of tumour cells, i.e., tumour cells with oxygen enrichment but less efficient in aerobic glycolysis. According to "Warburg effect," the tumour cell produces ATP at a low rate and uses glucose uptake for aerobic glycolysis to generate energy [5]. The final and physiologically irreversible phase of glycolysis, the conversion of phosphoenolpyruvate (PEP) to pyruvate through the addition of a phosphate group to ADP, is catalysed by the enzyme pyruvate kinase (PK) [6]. PKM2 is an isoform of PK that is found in mammals and is often highly expressed during cancer regeneration and embryogenesis. PKM2 differs from PKM1, which has 22 distinct amino acids. As a result, it has a binding pocket for fructose-1,6-bisphosphate and must rely on allosteric binding of FBP to produce an active tetramer [7]. PKM2 may also be crucial in sustaining the metabolic pathway of cancer cells. PKM2's enzymatic activity may also be suppressed by binding to tyrosine phosphorylated proteins, establishing a relationship between decreased PKM2 activity and phospho-tyrosine mediated growth signalling [8]. PKM2 is activated by their substrate, PEP, as well as the upstream glycolytic intermediate FBP. The thyroid hormone T3 inhibits PKM2 in the body [9]. Additionally, PKM2 has several special allosteric effectors that activate the enzyme's activity, including serine and SAICAR, a step in the manufacture of *de novo* purines [10].

The rapid computational advancements and algorithms have significantly improved the screening of drugs or their design, resulting in notable reductions in both time and costs associated with drug development. Typically, bioinformatics plays a crucial role in identifying key genes within extensive genomic data [11,12], providing probable target proteins to screen the suitable drug candidate. Biomolecular simulations, utilizing multiscale models, facilitate the investigation of thermodynamic and structural aspects of target proteins at various levels [13]. This exploration proves valuable for identifying the drug binding sites and deciphering drug's mechanisms of action. Following this, virtual screening examines chemical libraries to suggest potential candidates as drug based on the binding sites in target proteins [14,15]. Apart from virtual screening, *de novo* drug design approaches [16] that gives synthesizable molecules with high affinity to target proteins, also offer an alternative approach to the computer-aided drug design. Notably, artificial intelligence, encompassing deep learning and machine learning, is assuming increasingly key positions in computational methods, thereby influencing drug development [17,18]. Genetic regulatory networks (GRNs) have found successful applications in gene sequencing, particularly in processes involving the recognition of DNA and RNA [19,20].

Zanthoxylum armatum is a tall and evergreen plant which are distributed in southwest China and some regions of Southeast Asia [21]. The leaves of this plant are eaten as a seasoning and are traditionally used for the treatment of various diseases like headache, fever, and inflammation [22–24]. Different parts of *Z. armatum* such as fruit berries are used for the treatment of abdominal pain, skin diseases, and rheumatism, and as antispasmodic and carminative [25]. The plant is used by pharmaceutical companies for toothpaste production and used to cure toothache and against gum bleeding [26,27]. The seeds of this plant are also used as an aromatic tonic for certain conditions like fever, stomach ache, dyspepsia, etc. [24,25]. Moreover, it treats inflammation, fever, and low blood pressure [28]. *Z. armatum* harbours numerous alkaloids, including b-fagarine, g-fagarine, magnoflorine, chelerythrine, nitidine, tambatarine, etc [29]. Additionally, it contains linalool, tamblin, beta-sitosterol, aramatamide, tambulatin, lignans, fragesin, and asarinin. Within the plant's bark, the crystalline berberine has also been reported [30]. Extensive chemical studies have been conducted, unveiling the isolation of many novel phenolic compounds [29]. Furthermore, the stems of *Z. armatum* yielded the isolation of two new phenolic glycosides [31].

Herein, we used computational tools to check the toxicity, anticancer, and pharmacokinetic properties of various phytocompounds associated with *Z. armatum* of which the molecular target was PKM2. The molecular dynamics simulations were performed to assess the stability, intermolecular interactions between the ligands and PKM2 and, the conformational changes in PKM2. The lead compounds need further in vitro and in vivo examinations for the development of effective anticancer therapeutic agents.

2. Experimental section

2.1. Preparation of the phytocompounds of Zanthoxylum armatum

The SDF format files of the 3D structure of phytocompounds of *Zanthoxylum armatum* were obtained from PubChem. A total of 96 compounds of this plant were cured from the literature that is included in this study [32–35]. The basic details such as the PubChem CID and molecular formula are enlisted in Supplementary Information, Table S1.

2.2. Assessment of ADMET properties

The parameters viz., absorption, distribution, metabolism, excretion, and toxicity (ADMET) of phytocompounds were determined with the help of pkCSM server [36]. ADMET properties provide valuable information that can be used to define the integrity and efficiency of phytocompounds during the early stages of compound selection. The evaluation of toxicity is one of the most important and crucial aspects of drug design and discovery [37].

2.3. Prediction of anticancer potential

Using the PASS-Way2Drug server, the assessment of the anticancer characteristics of the compounds was investigated. According to the similarity metrics that determine whether anticancer activity is expected to be highly probable or less likely, PASS provides p values [38].

2.4. Retrieval and preparation of PKM2 structure

The crystal structure of PKM2 produced by X-ray diffraction having resolution of 0.203 nm was obtained from Protein Data Bank (PDB ID: 3BJF). The homo-tetramer human PKM2 protein has 228.50 kDa molecular weight. PKM2's monomeric structure was used for investigations using molecular docking and molecular dynamics simulations.

2.5. Virtual screening of phytocompounds

A catalytic site is present in the active site of enzyme proteins, pocket in which substrate binds and reaction is catalysed to produce the product. Tetrameric protein PKM2 from mammals has four identical subunits. All monomers have one active site and are made up of a short N-terminal domain as well as three major domains A, B, and C. One of the well-known virtual screening methods is molecular docking, which determines the way of ligand binding to proteins. AutoDock Vina was used to do the molecular docking [39]. Prior to processing, the receptor molecule, i.e., PKM2, was properly cleaned by removing all non-PKM2 coordinates. After adding the non-polar hydrogen, Kollman charges were added. The grid's spacing was set at 1 Å. The grid's dimensions were $54 \times 64 \times 86$ Å, and its centre was located at $x = 3.580$, $y = -18.461$, and $z = 27.361$. Using AutoDockTools-1.5.6, PKM2 structure was eventually saved as PDBQT file. To achieve the optimal conformation, the compounds were made flexible in AutoDockTools-1.5.6. The ligands were saved in PDBQT format. LigPlot^{+}, Discovery Studio 2021, and PyMOL were used to examine the molecular docking results.

2.6. Molecular dynamics

Molecular dynamics (MD) simulations were performed for further investigation of the top three compounds (nevadensin, asarinin, and kaempferol) displaying the lowest binding energy against PKM2. The docked conformations with the lowest energies for these compounds were used as the starting structure for the molecular simulations using the amber99sb-ILDN force field in the Gromacs 2018.1 package [40,41]. With the help of the Antechamber package of AmberTools21, the ligands' topology was created [42]. As a control, PKM2 alone was also simulated. TIP3P water model was used to solvate all systems in a triclinic box, and then they were all neutralized by adding three chlorine ions. 150 mM NaCl was also added to the system to mimic the physiological salt concentration. The weak van der Waals interactions were eliminated minimizing the system's energy up to a maximum of 50,000 steps. NVT equilibration was done for 1000 ps using the V-rescale thermostat at physiological temperature (310 K) [43]. NPT equilibration was completed with the Parrinello-Rahman barostat for another 1 ns at 1.0 bar [44]. The 100 ns MD simulations were eventually run on the equilibrated structure. Periodic boundary conditions (PBC) corrections were applied to all trajectories before analysis. Root-mean-square deviation (RMSD) of backbone atoms was calculated using the Gromacs program. Calculations were also made for the root-mean-square fluctuations (RMSF), solvent-accessible surface area (SASA), radius of gyration (R_g), hydrogen bond analysis, secondary protein structure, etc. Principal complement analysis was done using gmx cover utility of Gromacs. MM-PBSA computation was used to evaluate the energetics of the complexation of lead compounds with PKM2 [45].

3. Results and discussion

3.1. ADMET properties prediction

Using in silico methods, a preliminary examination of phytocompounds from *Zanthoxylum armatum* was done to determine their potential toxicity in several models. Computer-aided toxicity studies, compared to traditional procedures, are quick and affordable tools to eliminate the potentially dangerous chemical compounds at an early stage and minimize many experiment assays. The pkCSM server was used to forecast the toxicity of each phytocompound. Supplementary Information, Table S2 provides details regarding the toxicological behaviour of compounds on different models of toxicity.

The mutagenic potential of a substance is measured by AMES toxicity [46]. One-hydroxy-6, 13-anthraquinone, berberine, dictamnine, fargarine, haplopine, nitidine, robustine, sanguinarine, skimmianine, asarinin, L-asarinin, sesamin, and dictamnine exhibited AMES toxicity. Six substances were anticipated to be positive in the hepatotoxicological assessment: alpha-pinene, umbelliferone, armatamide, cuminic aldehyde, *cis*-9, 12-octadecadienoic, and *cis*-9, 12, 15-octadecatrienoic acid. Almost all drugs displayed very low or insignificant toxicity when predicted using the *T. pyriformis* toxicity model, except for 2-tridecanone and (E)-Nerolidol [47]. This suggests that the majority of the investigated chemicals were not harmful to *T. pyriformis*. hERG-1 (human ethera-go-go-related gene 1) K^{+} channels, are not inhibited by any of the compound in this study. Since it can cause deadly cardiac arrhythmias, hERG-1 is poisonous to the heart. To lessen cardiotoxicity, early-stage identification of potential hERG inhibitors may also be crucial. Similarly, numerous compounds showed skin sensitivity. Additionally, acute oral toxicity in rats was also assessed. The majority of the phytocompounds in *Z. armatum* were not found to be hazardous. The ADME properties of the compounds are listed in Supplementary Information, Table S3. As evident from the data, ADME properties of compounds predicted by pkCSM web server show most of the compounds have favourable pharmacological properties.

3.2. Prediction of anticancer activity

Prior to docking, the PASS Online program was used to determine the probable cellular targets of the phytocompounds of *Z. armatum*. We solely predicted the anticancer efficacy using PASS Online, taking into account the two key factors of pyruvate kinase

inhibition and antineoplastic characteristics. Because the main objective of this study is to screen drugs against pyruvate kinase, these two criteria were chosen. The biological activities of substances are predicted by the PASS Online server, which then presents the results as biological activity (P_a) or inactivity indices (P_i) [38]. The list of compounds of *Z. armatum* with pyruvate kinase inhibition and antineoplastic activities is listed in Supplementary Information, Table S4. The P_a values of majority of phytocompounds were greater than Pi for antineoplastic properties, indicating a higher likelihood of biological activity compared to inactivity. These two characteristics indicate that these compounds have a higher likelihood of anticancer action. It is documented that compounds of *Olea europaea* were predicted for anticancer potential through the PASS server of Way2Drug in which several compounds were found to be effective in pyruvate kinase inhibition and ultimately being antineoplastic [48].

3.3. Virtual screening of phytocompounds of Z. armatum

The molecular docking was carried out to get the interaction of phytocompounds with PKM2 that it also served as an important parameter for virtual screening. Using AutoDock Vina software, the compounds from *Z. armatum* were docked. The conformations with the lowest binding energy along with the inhibition constants for PKM2 are summarized in Supplementary Information, Table S5.

The majority of compounds displayed strong binding affinities for PKM2, where binding energies were found in the range of −5.1 to −9.7 kcal/mol. Out of 96 compounds, 26 were discovered to be at PKM2's catalytic site when docked with AutoDock Vina. Five phytocompounds were docked at allosteric site, while the remaining compounds interacted at the places other than catalytic and allosteric sites. Nevadensin, asarinin, and kaempferol were the top three substances identified based on a combination of factors including binding site, energy, pharmacokinetics properties, ADMET characteristics, and the predicted anticancer potential. It is noteworthy that the three lead compounds docked in PKM2's catalytic site. Nevadensin, asarinin, and kaempferol were determined to have inhibition constants of 1.606, 0.817, and 2.25 μmol/l, respectively. The result demonstrates how effective these drugs are at inhibiting PKM2 even at very low concentrations. Through hydrogen bonding, nevadensin interacted with PKM2's Ser362, Lys270, and Arg73 (Fig. 1A–C). Nevadensin interacts with Asp178 via hydrophobic forces. Similar hydrogen bonds were established by asarinin with Arg120 and Asn75 of PKM2 (Fig. 2A–C). Hydrophobic interactions involved more amino acids. Kaempferol was discovered to form hydrogen bonds with the following: Asn75, Gly295, Glu332, Arg73, and Lys270 (Fig. 3A–C). The findings are in agreement with previous reports where epicatechin, apigenin, and kaempferol interacted at the active site of PKM2 with binding energies of −8.0, −7.7, and −7.6 kcal/mol [49].

The interaction of hit compounds of this study at the active site might be responsible for the inhibition of enzymatic activity of PKM2 and ultimately exhibiting anticancer potential. A study has documented that rutin interacted with many amino acids of PKM2 such as Asp296, His78, Glu332, Arg73, and Arg120 of PKM2 via hydrogen bonds [48]. The evidence clearly demonstrates that these compounds have a high affinity for PKM2, which opens the door to further investigation of their therapeutic applications in both in vivo and in vitro settings.

3.4. Molecular dynamics simulation

3.4.1. Analysis of RMSD and RMSF

The RMSD of each system with respect to each of their initial conformations was calculated as part of preliminary examination of molecular simulation data. The RMSD values give a general notion of how stable proteins and complexes are during MD simulation investigations. In Fig. 4A, the RMSD for all systems is presented. Up to 40 ns, the RMSD of all systems showed some fluctuations before becoming stable. This demonstrates that after 40 ns, all systems were properly equilibrated [50]. PKM2 alone was found to have an average RMSD of 0.340 nm. Similarly, it was discovered that the RMSD of PKM2-nevadensin complex, PKM2-asarinin complex, and PKM2-kaempferol complex was 0.397, 0.413, and 0.233 nm, respectively.

A similar finding has been reported where the RMSD of PKM2 alone, PKM2-luteolin_7_O_glucoside complex, PKM2-rutin complex, and PKM2-verbascoside complex was less than 0.5 nm during 100 ns MD simulation [48]. By computing the RMSF of C_α atoms of residues (Fig. 4B), fluctuations in restudies of PKM2 alone and the complexes was investigated. RMSF of most amino acids was discovered to be less than 0.25 nm, further demonstrating the system's stability. The coils and loops of PKM2, which fluctuate in

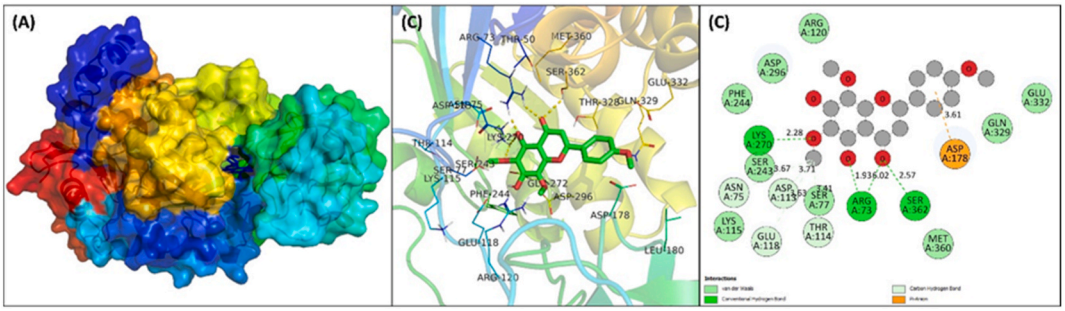

Fig. 1. Docked pose of PKM2-nevadensin complex. (A) PKM2 is shown in coloured surface; nevadensin is shown in blue sticks at active site. (B) Interacting resides of PKM2 with nevadensin. (C) Two dimensional interaction plot of PKM2-nevadensin complex.

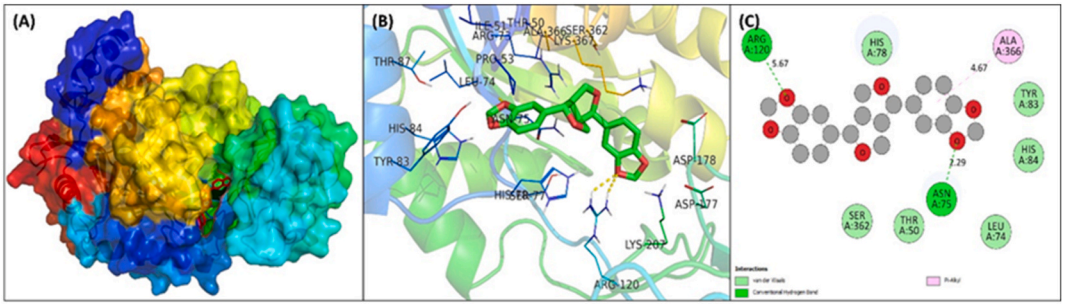

Fig. 2. Docked pose of PKM2-asarinin complex. (A) PKM2 is shown in coloured surface; asarinin is shown in red sticks at active site. (B) Interacting resides of PKM2 with asarinin. (C) Two dimensional interaction plot of PKM2-asarinin complex.

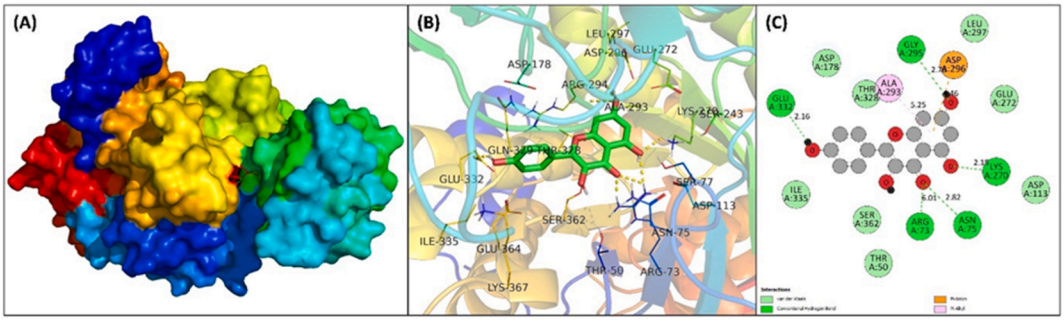

Fig. 3. Docked pose of PKM2-kaempferol complex. (A) PKM2 is shown in coloured surface; kaempferol is shown in red sticks at active site. (B) Interacting resides of PKM2 with kaempferol. (C) Two dimensional interaction plot of PKM2-kaempferol complex.

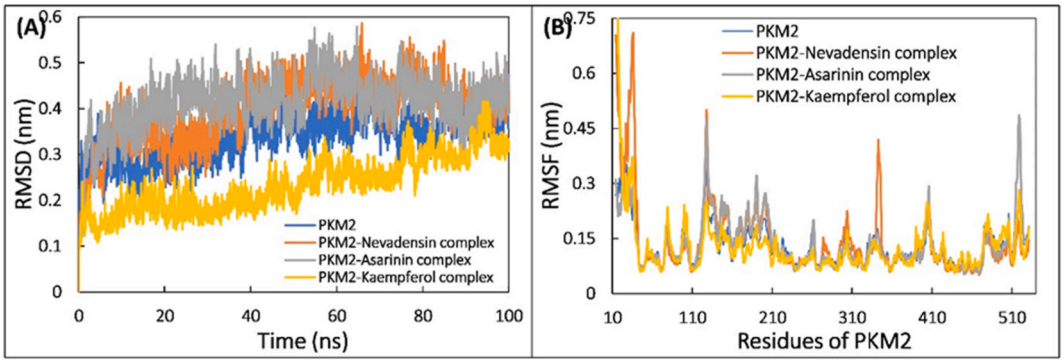

Fig. 4. (A) Root-mean square deviation of PKM2 alone, PKM2-nevadensin complex, PKM2-asarinin complex, and PKM2-kaempferol complex as function of time. (B) Root-mean square fluctuation in residues of PKM2 in the absence and presence of ligands (nevadensin, asarinin, and kaempferol).

aquatic surroundings, are considered responsible for some of the spikes in RMSF [51]. To determine the dynamic behaviour of all ligands, atom wise RMSF was determined (Supplementary Fig. S1). Asarinin was discovered to have the maximum dynamic behaviour out of all ligands, indicating their dynamic tendency in binding pocket. Nevadensin and kaempferol displayed substantially lesser variations. The rotatable bonds and movement at the binding site may be responsible for this dynamic behaviour. The docking tests showed that the binding sites were in PKM2's catalytic site. Throughout the entire simulation, all ligands remained in the active site, further confirming the binding and stable nature of complexes.

3.4.2. Analysis of compactness, physicochemical parameters, and secondary structure

To examine the stability of each, its physicochemical properties such as total energy and potential energy were calculated (Supplementary Fig. S2). All complexes maintained constant potential energies that was equal to the PKM2 by itself. The total energy of every system was also discovered to remain constant throughout the experiment. These variables reflect the system's stability under

physiological settings. The radius of gyration (R_g) is the mass-weighted RMS distance of a group of atoms from their common centre of mass. When compared to proteins in their expanded state, compact proteins, like globular proteins, typically have lesser radius changes in R_g [52]. In order to analyse the structural stability and compactness of proteins or complexes during MD simulation, the R_g values are considered to be a crucial metric [53]. Fig. 5A displays the R_g of PKM2 and its complexes.

PKM2 alone had an average R_g of 2.505 nm. Similar results were achieved for PKM2-nevadensin complex, PKM2-asarinin complex, and PKM2-kaempferol complex, which were determined to be 2.507, 2.532, and 2.444 nm, respectively. The information demonstrates how the complexes are stable. The finding is in agreement with the literature in which the average RMSD of PKM2-luteolin_7_O_glucoside complex, PKM2-rutin complex, and PKM2-verbascoside were found to be 2.458, 2.470, and 2.459 nm, respectively [48]. Additionally, SASA was computed as shown in Fig. 5B. SASA of apo PKM2 was 232.197 nm on average. PKM2-nevadensin complex, PKM2-asarinin complex, and PKM2-kaempferol complex exhibited average SASA as 236.000, 240.605, and 236.943 nm, respectively. The SASA of complexes showed minor changes compared to apo PKM2, and the consistency of results further verifies the stability of the systems under physiological conditions. A similar finding were reported earlier where average SASA of apo PKM2, PKM2-apigenin complex, PKM2-kaempferol complex, and PKM2-rutin complex was 233.26, 230.79, 236.51, and 235.55 nm^2, respectively [49]. Calculating the protein's secondary structure in both its complexed and uncomplexed states allowed researchers to examine the impact of ligand binding on the structural stability of PKM2, which showed each of the secondary structural parts of PKM2 and the complexes (Supplementary Fig. S3). It was discovered that PKM2 alone had 18.968, 1.05, 18.96, 11.90, 11.63, 34.21, and 3.25 percent of β-sheet, β-bridge, coils, turns, bends, α-helix, and 3′-helix, respectively. These values are consistent with literature where the percentage of coils, β-sheet, β-bridge, bends, turns, α-helix, and 3′-helices in PKM2 was 18.02, 19.81, 1.13, 11.81, 12.86, 32.92, and 3.42, respectively [48]. In the presence of each ligand, none of these PKM2 motifs underwent any noticeable change. For instance, average percentage of coils, β-sheet, β-bridge, bends, turns, α-helix, and 3′-helix in PKM2-nevadensin complex was 17.834, 20.238, 1.057, 2.135, 11.895, 33.113, and 3.724%, respectively. The structural integrity of every simulated complex is thus verified and eventually validated.

3.4.3. Examination of hydrogen bonding

All systems' hydrogen bond profiles were computed to analyse the interaction between text compounds and PKM2. Initially, hydrogen bond numbers as a function of time in the trajectory was determined (Fig. 6A). PKM2-nevadensin complex, PKM2-asarinin complex, and PKM2-kaempferol complex were shown to have average of 0.269, 0.363, and 1.912 hydrogen bonds, respectively. This demonstrates that compared to the other two ligands (nevadensin and asarinin), kaempferol formed more hydrogen bonds with PKM2.

The results are consistent with docking studies in which kaempferol demonstrated the highest affinity for PKM2. Hydrogen bonds were present during the whole simulation time, as evidenced by the examination of hydrogen bond profiles (Fig. 6B–D). The fact that the hydrogen bond profiles changed over time indicating that interactions between the ligands and PMK2 involved dynamic hydrogen bonds [54]. Additionally, there's a chance that the variations in hydrogen bonds are caused by interactions between water molecules at the binding site, which could change how the hydrogen bond profiles are distributed [55]. The hydrogen bond occupancy was also calculated. Lys367 showed the highest hydrogen bond occupancy in the PKM2-nevadensin complex. Similarly, Thr80 and Glu364 displayed the highest hydrogen bond occupancy in PKM2-asarinin complex and PKM2-kaempferol complex, respectively. Other residues of PKM2 were also involved in hydrogen bonds, but their occupancy was lower. In the binding of verbascoside and luteolin_7_O_glucoside to PKM2, Asn75 exhibited the highest occupancy of hydrogen bonds. Similarly, Glu364 showed the highest occupancy in the complexation of rutin to PKM2 [48].

3.4.4. Analysis of binding energy

MM-PBSA analysis were used to further analyse how the compounds interacted with PKM2. For this calculation, 100 frames at 1 ns interval were taken from each trajectory. Hydrogen bonds, electrostatic forces, hydrophobic forces, van der Waals forces, and other non-covalent forces dominate the interactions between proteins and ligands. The overall binding is either influenced positively or

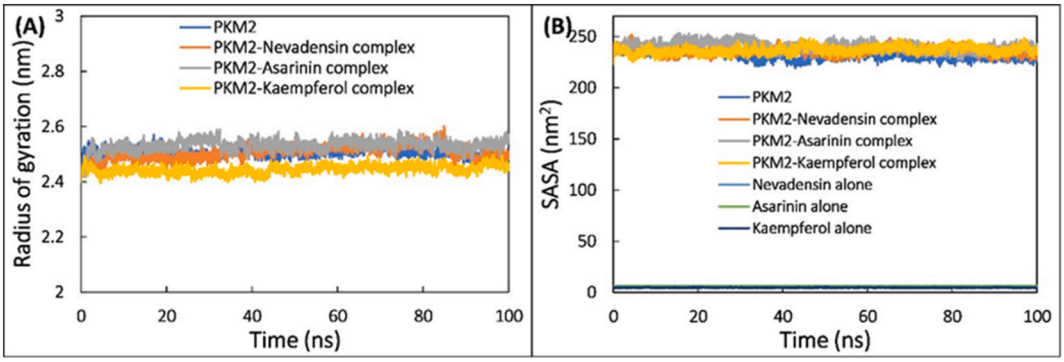

Fig. 5. (A) Radius of gyration of PKM2 alone, PKM2-nevadensin complex, PKM2-asarinin complex, and PKM2-kaempferol complex as function of time. (B) Solvent accessible surface area of gyration of PKM2 alone, PKM2-nevadensin complex, PKM2-asarinin complex, and PKM2-kaempferol complex as function of time.

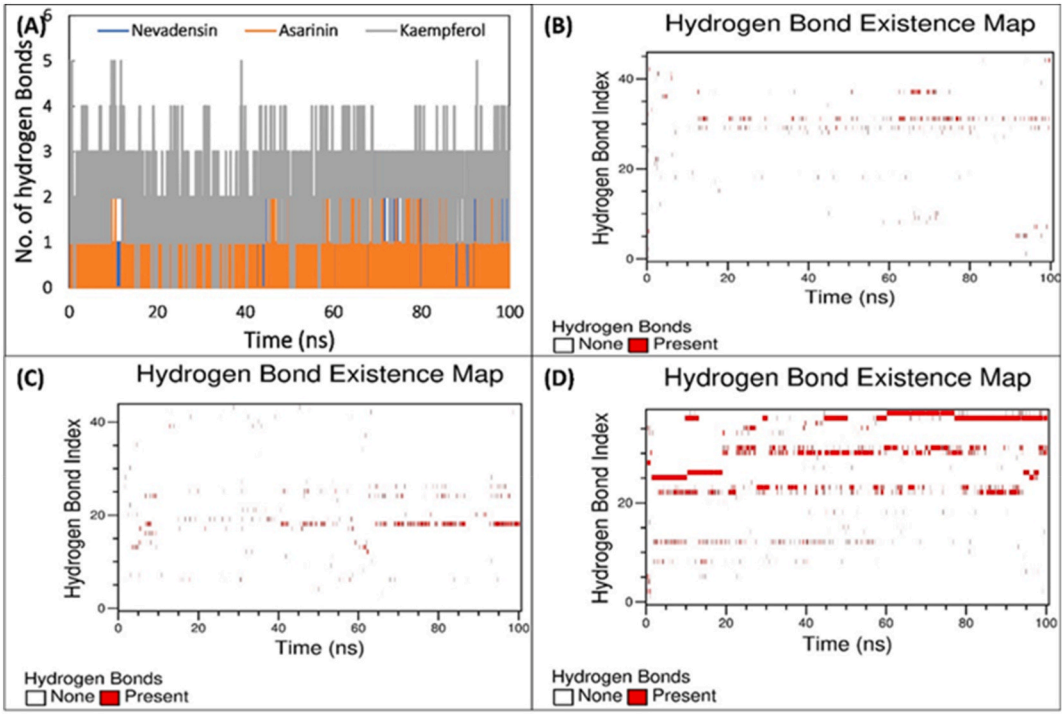

Fig. 6. (A) Humber of hydrogen bonds formed by nevadensin, asarinin, and kaempferol with PKM2 as function of time. (B) Hydrogen bond existence map of PKM2-nevadensin complex as function of time. (C) Hydrogen bond existence map of PKM2-asarinin complex as function of time. (D) Hydrogen bond existence map of PKM2-kaempferol complex as function of time.

negatively by these energies [56]. Using MM-PBSA, various binding energies were estimated (Supplementary Fig. S4). When ligands interact with PKM2, van der Waals and electrostatic forces predominated. The total binding energy also included a minor contribution from SASA energy. However, as can be seen from its positive values, the polar solvation energy hampered the overall binding of ligands to PKM2. Nevadensin, asarinin, and kaempferol were identified to interact with PKM2 with total binding energies of −20.210, −15.109, and −13.156 kcal/mol, respectively. A similar report is documented earlier where overall binding energy for the interaction of verbascoside, rutin, and luteolin_7_O_glucoside, with PKM2 calculated using MM-PBSA was −7.76, −15.00, and −3.22, kcal/mol, respectively [48]. Our findings are also quite close to the previous report where the binding energy for kaempferol and PKM2 complexation was with PKM2 was −12.865 kcal/mol [49].

Data from MM-PBSA analysis was further taken to identify the energy contribution of each residue of PKM2. The highest energy contributing residues for each ligand are listed in Table 1. Pro53, Thr50, Gly79, His78, Tyr83, Gly363, Ala366, and Lys367 of PKM2 were major energy contributors for interaction of nevadensin. In the PKM2-asarinin complex, Pro53, His78, Gly79, Thr80, Tyr83, His84, Lys224, and Lys367 were highest energy contributors. Likewise, in PKM2-kaempferol complex, Asp113, Asp178, Glu272, Thr328, Gln329, Glu332, Ile335, Glu344, and Glu364 residues showed the highest energy contribution. Some of these residues such as Gln329, Glu332, and Glu344 have been found to exhibit the highest energy contribution in complexation of kaempferol with PKM2 [49]. Polar energies of highest energy contributing amino acids were positive, indicating that polar energy of these amino acids hindered the overall binding. However, the negative values of the total energy of these residues are evidence of their positive interaction with the compounds. In the binding of verbascoside with PKM2, Thr50, Ser77, Pro53, Asp113, His78, Thr114, Val176, Glu118, Val209, 326, Asp177, Glu332, and Ala366 were reported as the highest energy contributors [48].

3.4.5. Principal component analysis

Principal component analysis (PCA) is a commonly used statistical method to examine the flexibility of proteins from molecular dynamics simulation data. PCA reduces the dimensionality of data sets without affecting the crucial information, which is represented as eigenvectors [48]. The flexibility of PKM2 without and with the ligands was analyzed using PCA and the eigenvector projection is shown in Fig. 7A.

PKM2 occupied a similar conformational space in the eigenvector's projection even after the complexation of ligands. A similar conformation space was also found earlier by PKM2 [48,49]. The data shows that the flexibility of PKM2 remained roughly the same in presence of ligands. PKM2-nevadensin complex and PKM2-asarinin complex showed slightly higher flexibility compared to PKM2 alone and PKM2-kaempferol complex. To further understand the patterns of PKM2's folding, free energy landscape (FEL) was prepared from eigenvector projection data. The (FEL) of apo PKM2 and the complexes are shown in Fig. 7B–D. It is interesting to note that all complexes and PKM2 alone reached the energy minima in their landscapes. However, the position of energy minima is slightly

Table 1
Apolar, polar, and total binding energies of the major energy contributing residues PKM2 for their interaction with hit compounds.

Nevadensin			
Residues	Polar Energy	Apolar Energy	Total Energy
Thr50	−0.084 ± 0.007	−0.035 ± 0.004	−0.448 ± 0.035
Gly52	0.582 ± 0.021	−0.035 ± 0.002	−0.350 ± 0.025
Pro53	0.148 ± 0.027	−0.207 ± 0.006	−1.844 ± 0.059
Arg56	−0.239 ± 0.055	0.000 ± 0.000	−0.317 ± 0.044
Arg73	−0.272 ± 0.109	−0.008 ± 0.002	−0.327 ± 0.042
His78	2.236 ± 0.084	−0.370 ± 0.009	−1.645 ± 0.092
Gly79	0.417 ± 0.032	−0.109 ± 0.005	−0.520 ± 0.033
Tyr83	0.648 ± 0.030	−0.167 ± 0.007	−1.193 ± 0.068
Lys115	−0.374 ± 0.036	0.000 ± 0.000	−0.330 ± 0.033
Gly363	−0.038 ± 0.012	−0.036 ± 0.004	−0.355 ± 0.038
Ala366	0.047 ± 0.022	−0.072 ± 0.003	−0.859 ± 0.039
Lys367	3.146 ± 0.321	−0.205 ± 0.008	−0.456 ± 0.138
Asarinin			
Pro53	0.155 ± 0.033	−0.177 ± 0.010	−1.216 ± 0.063
Arg56	−0.179 ± 0.071	−0.001 ± 0.001	−0.301 ± 0.053
Arg73	−0.153 ± 0.019	0.000 ± 0.000	−0.173 ± 0.020
His78	1.588 ± 0.086	−0.224 ± 0.010	−0.593 ± 0.078
Gly79	0.880 ± 0.055	−0.127 ± 0.006	−0.628 ± 0.050
Thr80	0.861 ± 0.074	−0.138 ± 0.008	−0.596 ± 0.060
Tyr83	1.008 ± 0.044	−0.241 ± 0.011	−2.001 ± 0.096
His84	0.314 ± 0.053	−0.036 ± 0.004	−0.335 ± 0.036
Lys224	−0.100 ± 0.025	−0.001 ± 0.000	−0.257 ± 0.021
Lys270	−0.107 ± 0.013	0.000 ± 0.000	−0.124 ± 0.013
Ala366	−0.005 ± 0.017	−0.015 ± 0.003	−0.174 ± 0.025
Lys367	0.538 ± 0.132	−0.079 ± 0.010	−0.308 ± 0.085
Kaempferol			
Asp113	−1.034 ± 0.053	0.000 ± 0.000	−0.521 ± 0.056
Glu118	−0.454 ± 0.055	−0.003 ± 0.001	−0.352 ± 0.062
Asp177	−0.201 ± 0.056	0.000 ± 0.000	−0.359 ± 0.045
Glu300	0.084 ± 0.015	0.000 ± 0.000	−0.232 ± 0.014
Thr328	1.327 ± 0.078	−0.157 ± 0.004	−0.682 ± 0.053
Gln329	1.538 ± 0.077	−0.174 ± 0.006	−1.064 ± 0.064
Glu332	0.807 ± 0.170	−0.058 ± 0.003	−0.642 ± 0.094
Ile335	0.048 ± 0.006	−0.072 ± 0.004	−0.549 ± 0.033
Glu344	−0.329 ± 0.020	0.000 ± 0.000	−0.294 ± 0.017
Asp347	−0.342 ± 0.020	0.000 ± 0.000	−0.326 ± 0.017
Asp357	−0.242 ± 0.010	0.000 ± 0.000	−0.211 ± 0.008
Glu364	−0.485 ± 0.202	−0.023 ± 0.002	−3.110 ± 0.151

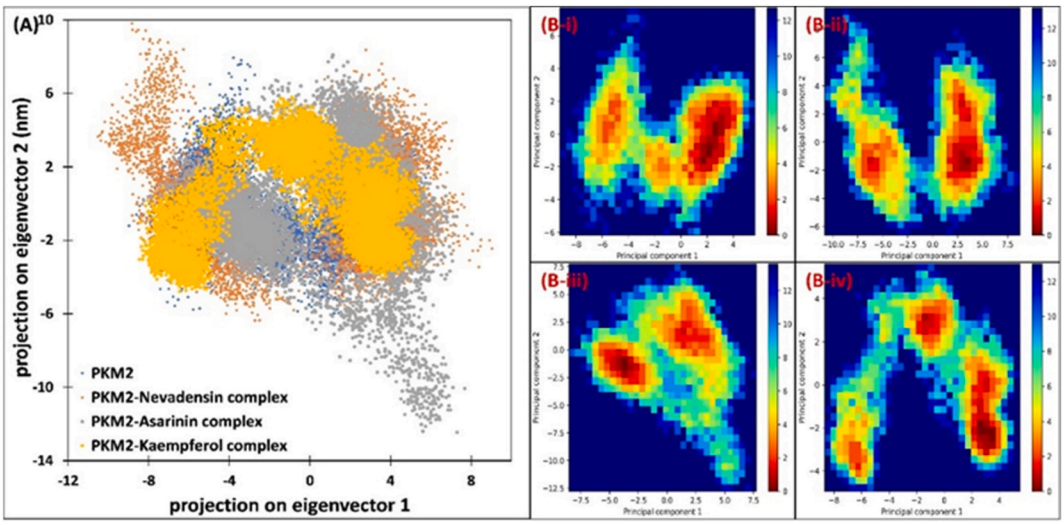

Fig. 7. (A) Projection of eigenvectors of PKM2 alone, PKM2-nevadensin complex, PKM2-asarinin complex, and PKM2-kaempferol complex. (B-i) Free energy landscape of PKM2 alone. (B-ii) Free energy landscape of PKM2-nevadensin complex. (B-iii) Free energy landscape of PKM2-asarinin complex. (B-iv) Free energy landscape of PKM2-kaempferol complex.

different for all systems. The detailed structural analysis of PKM2 was done by extracting the energy minima structures. The Ramachandran plots of energy minima coordinates are shown in Supplementary Fig. S5. Two amino acids were found in generously allowed region and only one was found in disallowed region of apo PKM2. Similar result was found for PKM2-nevadensin complex where the number of residues in generously allowed regions and disallowed regions was two and one, respectively. However, no residue was found in the generously allowed, and two residues lied in the disallowed region of PKM2-asarinin complex and PKM2-kaempferol complex. These differences are nominal. The presence of most of the residues in favoured regions and additional allowed regions for all complexes show that PKM2 did not undergo any abrupt or inappropriate structural changes during simulation.

4. Conclusions

PKM2 is a specific isoform of pyruvate kinase which is known to be involved in progression of certain cancers. Owing to its role in cancer, we have targeted PKM2 to screen the phytocompounds and identify the potential candidates. Plant-based compounds may prove effective in the discovery of anticancer medicines, especially from medicinal plants. The phytochemicals in *Z. armatum* might have good anticancer properties. By employing in silico methods, we found nevadensin, asarinin, and kaempferol as the top compounds from *Z. armatum*, having higher binding affinities towards PKM2, exhibiting inhibition constants as 1606, 817, and 2251 nM, respectively. The ligands interact at the PKM2's catalytic site. Additionally, hit compounds have an enormous chance of inhibiting a protein, and their antineoplastic features suggest a high likelihood of anticancer efficacy. The robust binding of lead compounds to PKM2 protein is supported by the MM-PBSA calculations. Out of the three hit compounds, we cannot definitively say which one has the most potential based on the data because some of the compounds performed better than others in different aspects. Therefore, we suggest nevadensin, asarinin, and kaempferol as prospective lead chemicals for additional research in the therapeutic development against PKM2 to combat cancer.

Funding

This research is funded by Researchers Supporting Project number (RSPD2024R979), King Saud University, Riyadh, Saudi Arabia.

Data availability

Data will be made available on request.

CRediT authorship contribution statement

Mohd Afzal: Writing – original draft, Funding acquisition, Conceptualization. **Faizan Abul Qais:** Validation, Methodology, Investigation, Data curation, Conceptualization. **Naaser A.Y. Abduh:** Visualization, Methodology, Formal analysis. **Maria Christy:** Visualization, Data curation. **Rashid Ayub:** Writing – review & editing, Software, Data curation. **Abdullah Alarifi:** Supervision, Investigation.

Declaration of competing interest

The authors declare that they have no known competing financial interests or personal relationships that could have appeared to influence the work reported in this paper.

Acknowledgments

The authors extend their appreciation to Researchers Supporting Project number (RSPD2024R979), King Saud University, Riyadh, Saudi Arabia.

Appendix A. Supplementary data

Supplementary data to this article can be found online at https://doi.org/10.1016/j.heliyon.2024.e27361.

References

[1] D.T. Debela, S.G. Muzazu, K.D. Heraro, M.T. Ndalama, B.W. Mesele, D.C. Haile, S.K. Kitui, T. Manyazewal, New Approaches and Procedures for Cancer Treatment: Current Perspectives, vol. 9, SAGE Open Med, 2021 205031212110343, https://doi.org/10.1177/20503121211034366.

[2] A. Lichota, K. Gwozdzinski, Anticancer activity of natural compounds from plant and marine environment, Int. J. Mol. Sci. 19 (2018), https://doi.org/10.3390/ijms19113533.

[3] I.B. Abubakar, A.N. Ukwuani-Kwaja, A.D. Garba, D. Singh, I. Malami, T.S. Salihu, A. Muhammad, Y. Yahaya, S.M. Sule, S.J. Ahmed, Ethnobotanical study of medicinal plants used for cancer treatment in Kebbi state, North-west Nigeria, Acta Ecol. Sin. 40 (2020) 306–314, https://doi.org/10.1016/J.CHNAES.2020.02.007.

[4] K.E. Adewole, Nigerian antimalarial plants and their anticancer potential: a review, J. Integr. Med. 18 (2020) 92–113, https://doi.org/10.1016/j.joim.2020.01.001.
[5] P.W. Stacpoole, Therapeutic targeting of the pyruvate dehydrogenase complex/pyruvate dehydrogenase kinase (PDC/PDK) Axis in cancer, J. Natl. Cancer Inst. 109 (2017) 1–14, https://doi.org/10.1093/jnci/djx071.
[6] M.S. Jurica, A. Mesecar, P.J. Heath, W. Shi, T. Nowak, B.L. Stoddard, The allosteric regulation of pyruvate kinase by fructose-1,6-bisphosphate, Structure 6 (1998) 195–210, https://doi.org/10.1016/S0969-2126(98)00021-5.
[7] J.D. Dombrauckas, B.D. Santarsiero, A.D. Mesecar, Structural basis for tumor pyruvate kinase M2 allosteric regulation and catalysis, Biochemistry 44 (2005) 9417–9429, https://doi.org/10.1021/bi0474923.
[8] H.R. Christofk, M.G. Vander Heiden, N. Wu, J.M. Asara, L.C. Cantley, Pyruvate kinase M2 is a phosphotyrosine-binding protein, Nature 452 (2008) 181–186, https://doi.org/10.1038/nature06667.
[9] K. Ashizawa, P. McPhie, K. huei Lin, S. yann Cheng, An in vitro novel mechanism of regulating the activity of pyruvate kinase M2 by thyroid hormone and fructose 1,6-bisphosphate, Biochemistry 30 (1991) 7105–7111, https://doi.org/10.1021/bi00243a010.
[10] H.P. Morgan, F.J. O'Reilly, M.A. Wear, J. Robert O'Neill, L.A. Fothergill-Gilmore, T. Hupp, M.D. Walkinshaw, M2 pyruvate kinase provides a mechanism for nutrient sensing and regulation of cell proliferation, Proc. Natl. Acad. Sci. U. S. A. 110 (2013) 5881–5886, https://doi.org/10.1073/pnas.1217157110.
[11] X. Lin, X. Li, X. Lin, A review on applications of computational methods in drug screening and design, Molecules 25 (2020) 1375, https://doi.org/10.3390/molecules25061375.
[12] Y. Yamanishi, M. Araki, A. Gutteridge, W. Honda, M. Kanehisa, Prediction of drug–target interaction networks from the integration of chemical and genomic spaces, Bioinformatics 24 (2008) i232–i240, https://doi.org/10.1093/bioinformatics/btn162.
[13] G.S. Ayton, W.G. Noid, G.A. Voth, Multiscale modeling of biomolecular systems: in serial and in parallel, Curr. Opin. Struct. Biol. 17 (2007) 192–198, https://doi.org/10.1016/j.sbi.2007.03.004.
[14] S. Forli, R. Huey, M.E. Pique, M.F. Sanner, D.S. Goodsell, A.J. Olson, Computational protein–ligand docking and virtual drug screening with the AutoDock suite, Nat. Protoc. 11 (2016) 905–919, https://doi.org/10.1038/nprot.2016.051.
[15] A.R. Rosales, J. Wahlers, E. Limé, R.E. Meadows, K.W. Leslie, R. Savin, F. Bell, E. Hansen, P. Helquist, R.H. Munday, O. Wiest, P.-O. Norrby, Rapid virtual screening of enantioselective catalysts using CatVS, Nat. Catal. 2 (2018) 41–45, https://doi.org/10.1038/s41929-018-0193-3.
[16] G. Schneider, D.E. Clark, Automated de novo drug design: are we nearly there yet? Angew. Chemie Int. Ed. 58 (2019) 10792–10803, https://doi.org/10.1002/anie.201814681.
[17] P.J. Ballester, Machine learning for molecular modelling in drug design, Biomolecules 9 (2019) 216, https://doi.org/10.3390/biom9060216.
[18] M. Popova, O. Isayev, A. Tropsha, Deep reinforcement learning for de novo drug design, Sci. Adv. 4 (2018), https://doi.org/10.1126/sciadv.aap7885.
[19] Y. Cao, A. Chandrasekar, T. Radhika, V. Vijayakumar, Input-to-state stability of stochastic Markovian jump genetic regulatory networks, Math. Comput. Simul. (2023), https://doi.org/10.1016/j.matcom.2023.08.007.
[20] T. Radhika, A. Chandrasekar, V. Vijayakumar, Q. Zhu, Analysis of markovian jump stochastic cohen–grossberg BAM neural networks with time delays for exponential input-to-state stability, Neural Process. Lett. 55 (2023) 11055–11072, https://doi.org/10.1007/s11063-023-11364-4.
[21] S. Feng, L. Zhao, Z. Liu, Y. Liu, T. Yang, A. Wei, De novo transcriptome assembly of Zanthoxylum bungeanum using lllumina sequencing for evolutionary analysis and simple sequence repeat marker development, Sci. Rep. 7 (2017) 1–11, https://doi.org/10.1038/s41598-017-15911-7.
[22] J. Raju, V. C, Diosgenin, a Steroid Saponin Constituent of Yams and Fenugreek: Emerging Evidence for Applications in Medicine, 2012, https://doi.org/10.5772/26700.
[23] M.N. Mushtaq, S. Ghimire, Alamgeer, M.S. Akhtar, A. Adhikari, C. Auger, V.B. Schini-Kerth, Tambulin is a major active compound of a methanolic extract of fruits of Zanthoxylum armatum DC causing endothelium-independent relaxations in porcine coronary artery rings via the cyclic AMP and cyclic GMP relaxing pathways, Phytomedicine 53 (2019) 163–170, https://doi.org/10.1016/j.phymed.2018.09.020.
[24] Z. Nooreen, A. Kumar, D.U. Bawankule, S. Tandon, M. Ali, T.D. Xuan, A. Ahmad, New chemical constituents from the fruits of Zanthoxylum armatum and its in vitro anti-inflammatory profile, Nat. Prod. Res. 33 (2019) 665–672, https://doi.org/10.1080/14786419.2017.1405404.
[25] N. Phuyal, P.K. Jha, P. Prasad Raturi, S. Rajbhandary, Zanthoxylum armatum DC.: current knowledge, gaps and opportunities in Nepal, J. Ethnopharmacol. 229 (2019) 326–341, https://doi.org/10.1016/j.jep.2018.08.010.
[26] C.C. Attribution-noncommercial-sharealike, I. License, C.C. By-nc-sa, A. Trust, traditional uses and conservation of timur (Zanthoxylum armatum dc) through social institutions in Uttaranchal himalaya , India author (s): chandra prakash kala , nehal A . Farooquee and uppeandra dhar published by, Ashoka Trust for Res. Ecol. 3 (2005) 224–230.
[27] D. Mehta, R. Das, A. Bhandari, In-vitro anthelmintic activity of seeds of Zanthoxylum armatum DC. against Pheretima Posthuma, Int. J. Green Pharm. 6 (2012) 26–28, https://doi.org/10.4103/0973-8258.97116.
[28] H.P. Kayat, S.D. Gautam, R.N. Jha, GC-MS analysis of hexane extract of Zanthoxylum armatum DC. fruits, J. Pharmacogn. Phytochem. 5 (2016) 58–62.
[29] A. Paul, A. Kumar, G. Singh, A. Choudhary, Medicinal, pharmaceutical and pharmacological properties of Zanthoxylum armatum: a Review, J. Pharmacogn. Phytochem. 7 (2018) 892–900.
[30] L. Ranawat, J. Bhatt, J. Patel, Hepatoprotective activity of ethanolic extracts of bark of Zanthoxylum armatum DC in CCl4 induced hepatic damage in rats, J. Ethnopharmacol. 127 (2010) 777–780, https://doi.org/10.1016/j.jep.2009.10.019.
[31] H. Li, P. Li, L. Zhu, M. Xie, Z. Wu, Studies on the chemical constituents of Zanthoxylum armatum DC, Chinese Pharm. 17 (2006) 1035–1037.
[32] T. Singh, O. Singh, Phytochemical and pharmacological profile of Zanthoxylum armatum DC. -An overview, Indian J. Nat. Prod. Resour. 2 (2011) 275–285.
[33] F. Alam, K.M. Din, R. Rasheed, A. Sadiq, M.S. Jan, A.M. Minhas, A. Khan, Phytochemical investigation, anti-inflammatory, antipyretic and antinociceptive activities of Zanthoxylum armatum DC extracts-in vivo and in vitro experiments, Heliyon 6 (2020) e05571, https://doi.org/10.1016/j.heliyon.2020.e05571.
[34] G. Jothi, K. Keerthana, G. Sridharan, Pharmacognostic, physicochemical, and phytochemical studies on stem bark of Zanthoxylum armatum DC, Asian J. Pharm. Clin. Res. 12 (2019) 1–5.
[35] C. Choudhury Barua, N. Yasmin, R.E. Cheran, A review on effective utilization, phytochemical compounds, pharmacological intervention of a popularly used plant for developing a new drug: zanthoxylum armatum with reference to its anticancer activity, MOJ Bioequivalence Bioavailab 5 (2018), https://doi.org/10.15406/mojbb.2018.05.00097.
[36] D.E.V. Pires, T.L. Blundell, D.B. Ascher, pkCSM: predicting small-molecule pharmacokinetic and toxicity properties using graph-based signatures, J. Med. Chem. 58 (2015) 4066–4072, https://doi.org/10.1021/acs.jmedchem.5b00104.
[37] Y. Wang, J. Xing, Y. Xu, N. Zhou, J. Peng, Z. Xiong, X. Liu, X. Luo, C. Luo, K. Chen, M. Zheng, H. Jiang, In silico ADME/T modelling for rational drug design, Q. Rev. Biophys. 48 (2015) 488–515, https://doi.org/10.1017/S0033583515000190.
[38] D.A. Filimonov, A.A. Lagunin, T.A. Gloriozova, A.V. Rudik, D.S. Druzhilovskii, P.V. Pogodin, V.V. Poroikov, Prediction of the biological activity spectra of organic compounds using the pass online web resource, Chem. Heterocycl. Compd. 50 (2014) 444–457, https://doi.org/10.1007/s10593-014-1496-1.
[39] A. Allouche, Software news and updates gabedit — a graphical user interface for computational chemistry softwares, J. Comput. Chem. 32 (2012) 174–182, https://doi.org/10.1002/jcc.
[40] H.J.C. Berendsen, D. van der Spoel, R. van Drunen, GROMACS: a message-passing parallel molecular dynamics implementation, Comput. Phys. Commun. 91 (1995) 43–56, https://doi.org/10.1016/0010-4655(95)00042-E.
[41] G. Sanchez, Las instituciones de ciencia y tecnología en los procesos de aprendizaje de la producción agroalimentaria en Argentina, El Sist. Argentino Innovación Inst. Empres. y Redes, El Desafío La Creación y Apropiación Conoc. 14 (2013) 659–664, https://doi.org/10.1002/prot.
[42] A.W. Sousa da Silva, W.F. Vranken, Acpype - AnteChamber PYthon parser interfacE, BMC Res. Notes 5 (2012) 367, https://doi.org/10.1186/1756-0500-5-367.
[43] G. Bussi, D. Donadio, M. Parrinello, Canonical sampling through velocity rescaling, J. Chem. Phys. 126 (2007) 014101, https://doi.org/10.1063/1.2408420.
[44] M. Parrinello, A. Rahman, Polymorphic transitions in single crystals: a new molecular dynamics method, J. Appl. Phys. 52 (1981) 7182–7190, https://doi.org/10.1063/1.328693.

[45] R. Kumari, R. Kumar, A. Lynn, g_mmpbsa —a GROMACS tool for high-throughput MM-PBSA calculations, J. Chem. Inf. Model. 54 (2014) 1951–1962, https://doi.org/10.1021/ci500020m.
[46] C. Xu, F. Cheng, L. Chen, Z. Du, W. Li, G. Liu, P.W. Lee, Y. Tang, In silico prediction of chemical ames mutagenicity, J. Chem. Inf. Model. 52 (2012) 2840–2847, https://doi.org/10.1021/ci300400a.
[47] F. Cheng, J. Shen, Y. Yu, W. Li, G. Liu, P.W. Lee, Y. Tang, In silico prediction of Tetrahymena pyriformis toxicity for diverse industrial chemicals with substructure pattern recognition and machine learning methods, Chemosphere 82 (2011) 1636–1643, https://doi.org/10.1016/j.chemosphere.2010.11.043.
[48] F.A. Qais, S.Y. Alomar, M.A. Imran, M.A. Hashmi, In-silico analysis of phytocompounds of olea europaea as potential anti-cancer agents to target PKM2 protein, Molecules 27 (2022) 5793, https://doi.org/10.3390/molecules27185793.
[49] S. Ahmed, M. Tabish, Phytocompounds screening of Nigella sativa in terms of human cancer by targeting sphingosine kinase-1 and pyruvate kinase-M2: a study based on in silico analysis, J. Biomol. Struct. Dyn. (2023) 1–15, https://doi.org/10.1080/07391102.2023.2212773.
[50] R.T. Fouedjou, S. Chtita, M. Bakhouch, S. Belaidi, M. Ouassaf, L.A. Djoumbissie, L.A. Tapondjou, F. Abul Qais, Cameroonian medicinal plants as potential candidates of SARS-CoV-2 inhibitors, J. Biomol. Struct. Dyn. (2021) 1–15, https://doi.org/10.1080/07391102.2021.1914170.
[51] M. Ouassaf, S. Belaidi, S. Chtita, T. Lanez, F. Abul Qais, H. Md Amiruddin, Combined molecular docking and dynamics simulations studies of natural compounds as potent inhibitors against SARS-CoV-2 main protease, J. Biomol. Struct. Dyn. 40 (2022) 11264–11273, https://doi.org/10.1080/07391102.2021.1957712.
[52] F.A. Qais, T. Sarwar, I. Ahmad, R.A. Khan, S.A. Shahzad, F.M. Husain, Glyburide inhibits non-enzymatic glycation of HSA: an approach for the management of AGEs associated diabetic complications, Int. J. Biol. Macromol. 169 (2021) 143–152, https://doi.org/10.1016/j.ijbiomac.2020.12.096.
[53] S. Chtita, S. Belaidi, F.A. Qais, M. Ouassaf, M.M. AlMogren, A.A. Al-Zahrani, M. Bakhouch, A. Belhassan, H. Zaki, M. Bouachrine, T. Lakhlifi, Unsymmetrical aromatic disulfides as SARS-CoV-2 Mpro inhibitors: molecular docking, molecular dynamics, and ADME scoring investigations, J. King. Saud. Univ. Sci. 34 (2022) 102226, https://doi.org/10.1016/j.jksus.2022.102226.
[54] S. Siddiqui, F. Ameen, I. Jahan, S.M. Nayeem, M. Tabish, A comprehensive spectroscopic and computational investigation on the binding of the anti-asthmatic drug triamcinolone with serum albumin, New J. Chem. 43 (2019) 4137–4151, https://doi.org/10.1039/C8NJ05486J.
[55] K. Ding, H. Zhang, H. Wang, X. Lv, L. Pan, W. Zhang, S. Zhuang, Atomic-scale investigation of the interactions between tetrabromobisphenol A, tetrabromobisphenol S and bovine trypsin by spectroscopies and molecular dynamics simulations, J. Hazard Mater. 299 (2015) 486–494, https://doi.org/10.1016/j.jhazmat.2015.07.050.
[56] B. Rath, F.A. Qais, R. Patro, S. Mohapatra, T. Sharma, Design, synthesis and molecular modeling studies of novel mesalamine linked coumarin for treatment of inflammatory bowel disease, Bioorg. Med. Chem. Lett. (2021) 128029, https://doi.org/10.1016/j.bmcl.2021.128029.